



OPEN ACCESS

Inverted Ge islands in {111} faceted Si pits—a novel approach towards SiGe islands with higher aspect ratio

To cite this article: M Grydlik *et al* 2010 *New J. Phys.* **12** 063002

View the [article online](#) for updates and enhancements.

You may also like

- [Recipes for the fabrication of strictly ordered Ge islands on pit-patterned Si\(001\) substrates](#)
Martyna Grydlik, Gregor Langer, Thomas Fromherz *et al.*
- [Thermally induced morphology evolution of pit-patterned Si substrate and its effect on nucleation properties of Ge dots](#)
Hung-Ming Chen, Chieh-Hsiung Kuan, Yuen-Wuu Suen *et al.*
- [Fabrication of Nanometer-Scale Si Field Emitters Using Self-Assembled Ge Nanomasks](#)
Sheng-Wei Lee, Bo-Lun Wu and Hung-Tai Chang

Inverted Ge islands in {111} faceted Si pits— a novel approach towards SiGe islands with higher aspect ratio

M Grydlik¹, M Brehm, F Hackl, H Groiss, T Fromherz, F Schäffler
and G Bauer

Institut für Halbleiter- und Festkörperphysik, Johannes Kepler Universität Linz,
Austria

E-mail: martyna.grydlik@jku.at

New Journal of Physics **12** (2010) 063002 (8pp)

Received 23 December 2009

Published 2 June 2010

Online at <http://www.njp.org/>

doi:10.1088/1367-2630/12/6/063002

Abstract. A detailed study of the so far unexplored Ge island nucleation on Si (001) substrates patterned with {111} faceted pyramidal pits is reported. The pits are defined by an anisotropic wet-chemical etch through a SiN_x hard mask. Due to the self-limiting of the wet etch, an extremely uniform pit pattern is achieved. On these substrates, Ge layers were grown by solid source molecular beam epitaxy at various growth temperatures T_{Ge} . For $T_{\text{Ge}} = 550^\circ\text{C}$, Ge fills the pits in the form of inverted {111} pyramids with a rounded apex and a (001)-oriented top surface. These islands have aspect ratios much larger than upright pyramids and domes that are usually obtained on substrates with cylindrical pits fabricated by lithographic techniques and reactive ion etching. Based on the experimentally determined shape, three-dimensional (3D) energy level calculations in an envelop function approach have been performed for the inverted pyramids. They show that, due to the orientation of the pyramid square base along $\langle 110 \rangle$ directions, the overlap between the hole ground states and electron states confined to the Si conduction band valleys perpendicular to the growth direction is much larger than for upright SiGe domes and {105} pyramids. For elevated growth temperatures around 700°C , already a Ge coverage of five monolayers induces a strong Si transfer into the {111} pits, effectively converting them towards {1 1 10} faceted ones.

¹ Author to whom any correspondence should be addressed.

1. Introduction

Strain-driven island nucleation during epitaxial growth of lattice-mismatched semiconductors (e.g. Ge on Si, InAs on GaAs) has been observed on both plain and patterned substrates [1–8]. On plain substrates, islands nucleate on randomly distributed sites. The morphological island evolution depends on a subtle interplay between kinetics and thermodynamics set by the growth conditions [9]. The random character of the formation process results in a statistical distribution of island size and composition.

By predefining the nucleation sites of the islands, one statistically distributed degree of freedom of the island formation process—the distance between neighboring nucleating islands—is frozen. Several methods of determining the nucleation sites have been reported in the literature, including buried stressors [10, 11], pre-patterned SiO₂ layers [12], and pit- [4] and stripe-patterned substrates [13, 14]. In the Ge-on-Si island system, the control of the nucleation site has been shown to result in a narrowing of the statistical size distribution of domes [15] or pyramids [6] formed in the pits, as well as in a spectral narrowing of the island photoluminescence (PL) [6, 16].

In an attempt to further reduce the statistical variations of QD size and composition, in this work we investigated the growth of SiGe islands in extremely uniform pits. Such pits can be defined by self-limiting etch processes on large substrate areas. For a Si substrate, potassium hydroxide (KOH) or tetramethylammonium hydroxide (TMAH) are suitable anisotropic etchants exposing {111} faceted pits. Substantial over-etching for achieving excellent homogeneity over large areas is not a problem, since the etching effectively stops as soon as the tip of a pyramidal pit has been established. In the Ga(In)As/(Al)GaAs system it has been shown that uniform quantum dot ensembles, exhibiting superior electronic and optic properties, can be grown in {111} faceted pits [17, 18].

Besides the technological improvements offered by pyramidal pits, from a physical point of view they are promising since QDs obtained by filling these pits would ideally have a very large aspect ratio of 0.71 (defined by the ratio between QD height and the square root of the QD base area), which can eventually result in *ordered* SiGe QDs with real three-dimensional (3D) quantization. The up to now smallest, perfectly ordered SiGe islands were demonstrated in [19] on templates structured by extreme ultraviolet interference lithography and reactive ion etching (RIE). These islands are {105} faceted pyramids with a height of only 3.6 nm. However, due to their shallow side facets (i.e. their small aspect ratio), their lateral extension ($36 \times 36 \text{ nm}^2$ base area) is still too large to achieve zero-dimensional quantum confinement in these pyramids.

2. Sample preparation and experimental results

In this work, the {111} faceted pyramidal pits were defined on (001) oriented, high-resistivity ($>3000 \Omega \text{ cm}$, p-type) Si substrates. 70 nm SiN_x layers were deposited on the substrates in a plasma enhanced chemical vapor deposition reactor. Regular pit arrays aligned along the $\langle 110 \rangle$ direction were defined by electron beam lithography. A H₂/CF₄ plasma in an RIE process is used to transfer the pit pattern into the SiN_x layer that hereafter is used as a hard mask for anisotropic etching of Si in TMAH at 80 °C. Since the etch rate in the Si $\langle 001 \rangle$ direction is $\sim 0.3 \mu\text{m min}^{-1}$ and the one for the Si $\langle 111 \rangle$ direction is as small as $\sim 0.01 \mu\text{m min}^{-1}$ [20], pits with well-defined {111} side facets result. The width and, thus, the depth of these pits are determined by the size of the hard mask openings. For the samples reported in this work, the

typical dimensions of the pits after all the fabrication steps are $\sim 200 \times 200 \text{ nm}^2$ base area and a corresponding depth of 140 nm.

On such substrates, first a Si buffer and then Ge is deposited by solid source molecular beam epitaxy (MBE). In the following, we compare the results obtained on substrates with different pit periods, as well as obtained by depositing various amounts of Ge at different growth temperatures. After *in situ* oxide desorption at 700°C for 45 min, for all samples a 45 nm thick Si buffer layer was grown at a rate of 0.06 nm s^{-1} . During buffer layer growth, the temperature was ramped up from 450 to 550°C . A series of samples at different growth temperatures (T_{Ge}) of the subsequent Ge layer ($T_{\text{Ge}} = 550, 625, \text{ and } 700^\circ\text{C}$) was grown at a Ge growth rate of $R_{\text{Ge}} = 0.005 \text{ nm s}^{-1}$. For optical investigations the samples were capped with 50 nm of Si at low enough temperature (300°C) to avoid intermixing, segregation and shape transformations during capping [21].

The surface morphology of the samples after different stages of the island growth was investigated by atomic force microscopy (AFM). Figure 1(a) displays the patterned surface after 45 nm Si buffer growth on a sample with a 350 nm pit period. During buffer growth, the edges of the pits are smoothed by the formation of $\{113\}$ facets; however, the $\{111\}$ orientation of the pit side facets remains unchanged. This is in sharp contrast to what is observed for cylindrical pits defined by RIE that develop shallow $\{110\}$ facets after Si buffer growth [22, 23]. Since for all $\{111\}$ pit-patterned samples investigated in this work the Si buffer was grown as described above, the pit shape shown in figure 1(a) is assumed as a starting point for Ge deposition under the different growth conditions described in the following.

After 4.8 monolayer (ML) Ge deposition at $T_{\text{Ge}} = 550^\circ\text{C}$, a flattening of the sharp pyramid tip obtained after Si buffer growth is observed in the AFM image (see figure 1(b)). The inset of figure 2 shows a cross section along a $[110]$ direction through a pit after Ge deposition, as measured by transmission electron microscopy (TEM). In order to highlight some of the faint signatures in the TEM picture without superimposing it, a schematic sketch is also shown in the inset. Clearly, the observed contrast at the pit apex indicates that Ge is preferentially growing there and forms a (001) top facet. Whether or not a Ge wetting layer (WL) is present cannot be concluded from the TEM pictures; however, from surface energy density calculations an approximately 2 ML thick WL can be expected [9, 24]. The boundary between the Si buffer and the island appears to be smeared out. Due to this smearing, the observed aspect ratio is smaller than the ideal one for $\{111\}$ pyramids; however, the observed aspect ratio of 0.41 (58 nm base width of top facet, height: 24 nm) is nevertheless the largest reported so far in the literature for SiGe islands with sub-500 nm dimensions grown on both planar and patterned substrates. For none of the inverted pyramids, dislocations were found in the TEM micrographs.

We want to emphasize that for substrates with $\{111\}$ pyramidal pits, perfect ordering of Ge islands is obtained at growth temperatures too low for ordered Ge nucleation on substrates patterned by cylindrical, RIE-etched pits with comparable period, on which $\{110\}$ faceted pits form during Si buffer growth. Figure 1(c) shows that for these substrates hut clusters nucleate around and between the shallow $\{110\}$ pits at 550°C growth temperature. On planar substrates used in the same growth run as a reference, hut cluster formation is observed (3 nm height), as shown in figure 1(d). Thus, for Ge growth on $\{111\}$ pyramidal pit-patterned substrates, the observed perfect filling indicates strong enhancement of Ge surface transport at a rather low growth temperature of 550°C . A similar behavior has been observed for the growth of $\text{Al}_x\text{Ga}_{1-x}\text{As}$ on $\{111\}$ pit-patterned GaAs substrates and has been ascribed to the capillarity effect [18]. Presumably this is also the process responsible for $\{111\}$ pyramidal pit filling in the SiGe system [25].

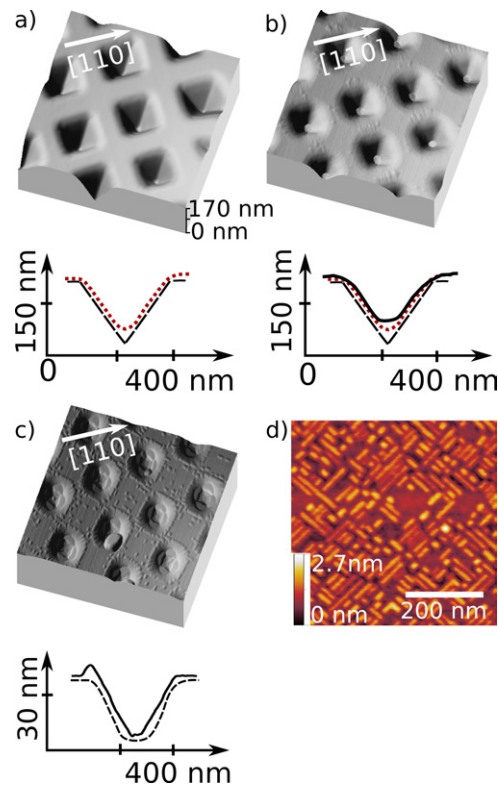


Figure 1. (a–c): 3D AFM images showing the morphology of a $1 \times 1 \mu\text{m}^2$ area on prestructured Si substrates (350 nm period), after (a) 45 nm of Si buffer growth, (b) additional 4.8 ML Ge grown at $T_{\text{Ge}} = 550^\circ\text{C}$ in $\{111\}$ inverted pyramid pits, and (c) 6 ML Ge grown at 550°C on top of a Si buffer in RIE-etched pits. The length of the height axis in all pictures corresponds to 170 nm. The arrows indicate the $[110]$ directions. Below the AFM images, the corresponding schematic AFM line scans are presented, where the broken lines indicate the original shape of the pit after wet etching ((a) and (b)) and plasma etching (c), and the red dotted line indicates the Si buffer layer surface ((a) and (b)). The solid lines are AFM line scans through the pit after Ge growth. (d) $500 \times 500 \text{ nm}^2$ AFM scan of hut clusters grown at $T_{\text{Ge}} = 550^\circ\text{C}$ on the planar regions of the sample.

Enhanced SiGe intermixing at $T_{\text{Ge}} = 550^\circ\text{C}$ is also evident from a comparison of the PL spectra emitted by Ge hut clusters nucleated outside the patterned region and the islands in the pyramidal pits shown in figure 2. The PL was excited by a frequency-doubled Nd:YAG laser (532 nm wavelength, power density of 1 kW cm^{-2}) and measured at 10 K through a microscope objective from an $\sim 30 \mu\text{m}$ diameter area within and outside the patterned substrate area. The sharp lines shown in figure 2 at 0.925 eV and at 1.1 eV are a laser line and the Si substrate PL, respectively. Between 0.85 and 1 eV, the island emission from the planar (hut cluster) and patterned (inverted pyramids) areas are shown. The hut cluster luminescence (figure 2, blue line) consists of two peaks corresponding to the no-phonon (0.94 eV) and phonon-assisted exciton recombination (0.89 eV), where the observed high emission energies are due to the small island

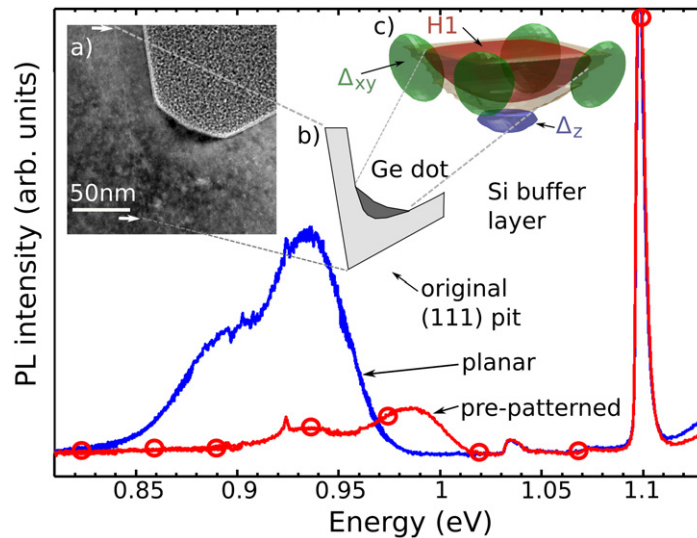


Figure 2. PL spectra from SiGe inverted pyramids nucleated during the deposition of 4.8 ML Ge at 550 °C (line with superimposed symbols). As a comparison, the hut cluster PL from the planar part of the sample is shown by the line without symbols. Insets: (a) TEM cross-sectional image through the tip of a {111} pit and (b) a schematic sketch of it. (c) Results of 3D energy level calculations based on the *nextnano*³ code [28] for a Si_{0.75}Ge_{0.25} island within an inverted pyramidal pit with structural parameters taken from TEM. The spatial electron and hole distributions around and in the island (surface shown in gray) are indicated by the green, blue and red surfaces, respectively, within which virtually all carriers are enclosed. An energy of 0.96 eV is calculated for a transition between the Δ_z (blue) conduction band and the H1 hole (red) ground states. The green surfaces indicate the distribution of electrons in the energetically lowest Δ_{xy} state that is 26 meV higher in energy than the Δ_z state.

size and the resulting large confinement energies². However, the no-phonon and phonon-assisted emission lines of the islands grown in the inverted pyramidal pits are observed at even higher energies of 0.985 eV and 0.93 eV, respectively (figure 2, red line).

To estimate the Ge content in the islands, 3D energy level calculations based on the *nextnano*³ code [28] were performed for various Ge concentrations in the islands. These calculations are based on a $\mathbf{k} \cdot \mathbf{p}$ envelope function approach fully taking into account the strain tensor field around and in an island, the multi-valley nature of the conduction bands as well as the mutual coupling of the three valence bands of Si and Ge. The relevant material parameters for Si and Ge used in the calculations are given in [29]. Instead of the spherically averaged hole masses used in our previous work [6, 16, 29], here the Si and Ge Luttinger parameters $\gamma_{1,2,3}$ were used for correct inclusion of the valence band coupling. For the SiGe alloy, these parameters were obtained by the interpolation scheme suggested in [30] from the respective

² Compared to hut cluster PL spectra reported in literature [27, 28], the hut-cluster luminescence measured on the plane substrate regions are observed at unusual high energy. However, in control experiments using identical growth conditions as for the growth on the pit-patterned substrates, we observe a systematic increase in the hut-cluster emission energy from the values reported in the literature towards the spectrum shown in figure 2 as the Ge coverage is decreased. These results are beyond the scope of the current paper and will be published elsewhere.

values of Si and Ge. Results of this interpolation are shown in [31]. However, because of the large island size, the inclusion of the mutual valence band coupling induces only a small light-hole admixture (6%) to the dominantly heavy-hole (94%) ground state wave function as well as a change of the hole ground state energy by less than 5 meV as compared with the results obtained in the single-band heavy-hole approximation with spherically averaged effective mass. For the same reason, no significant confinement energies are calculated. Thus, the energetic position of the PL is mainly determined by the average Ge content. Assuming a Ge content of 25%, a PL transition energy between the electron and the hole ground state of 0.96 eV is calculated, in reasonable agreement with the experimental observations.

Up to now it is not clear which processes are the reason for the enhanced intermixing at the moderate growth temperature of 550 °C by which the Ge content in the islands is reduced to $\sim 25\%$. However, it has been shown that also islands nucleating in {1 1 10} faceted pits have a lower maximum Ge concentration than islands nucleating on planar substrates under otherwise identical growth conditions [32]. Thus, we conclude that {111} pits enhance intermixing processes even more effectively. The lower integrated PL intensity observed for the inverted pyramids as compared with the PL emitted by the hut clusters is ascribed to the much lower areal density of the former.

In inset (c) of figure 2, the calculated electron and hole distribution around and within the island are shown by blue (Δ_z electrons), green (Δ_{xy} electrons) and red (H1 hole ground state) surfaces, outside which the probability density of finding an electron or hole has decayed to below 3% of its maximum value inside the surface. Here, Δ_{xy} (Δ_z) denotes electron states originating from the Si- Δ -conduction band minima oriented perpendicular (parallel) to the growth direction. The surface of the island is shown in gray. The shape of the island was taken from AFM and TEM scans. We want to emphasize that, due to the pit orientation along $\langle 110 \rangle$ directions, the Δ_{xy} wave functions are located at the *corners* of the pyramid's base square. As a consequence of the concave confinement potential towards the interior of the pyramid, at this position the electrons have a much larger overlap with the heavy-hole state located within the pyramids than calculated for the case of {105} faceted pyramids in [6], where the Δ_{xy} states are aligned *along* the $\langle 100 \rangle$ base edges. However, since the Δ_z state is the electron ground state, the increased Δ_{xy} overlap is expected to increase the island's absorbance but not its PL efficiency.

Increasing the growth temperature to $T_{\text{Ge}} = 700$ °C, Ge growth in {111} pits resembles the scenario observed for island nucleation in RIE-etched pits. At 2.9 ML Ge coverage and $T_{\text{Ge}} = 700$ °C, the originally {111} faceted pyramidal pits become shallower by the formation of high index facets as shown in the 3D AFM image figure 3(a). The surface facet plot [33] in figure 3(b) shows that the dominant facets are those characteristic for barn ({105}, {113}, {15 3 23}, {20 4 23} and {23 4 20}) [26]. In figure 3(b) these facets oriented in certain directions are marked by symbols.

At 4.8 ML coverage, the pits are smoothed out to a large degree and—for a pit pattern period of 350 nm—approach the shape of the {1 1 10} pits observed after RIE etching and Si buffer layer growth (see figure 3(c)) [22, 23]. We want to point out that 4.8 ML Ge coverage corresponds to a Ge volume per pattern unit cell smaller than 5% of the pit volume after buffer growth. From the AFM images we calculate that approximately 50 ML of Si have to be transferred from the regions between the pits into them and strong intermixing of Si and Ge has to take place in order to fill up the pits to the degree shown in figure 3(c). For a larger pattern period of 400 nm, corresponding to 30% more Ge available per pit, we observe nucleation of *upright domes* inside the pits (Figure 3(d)), further highlighting the similarity of the smoothed

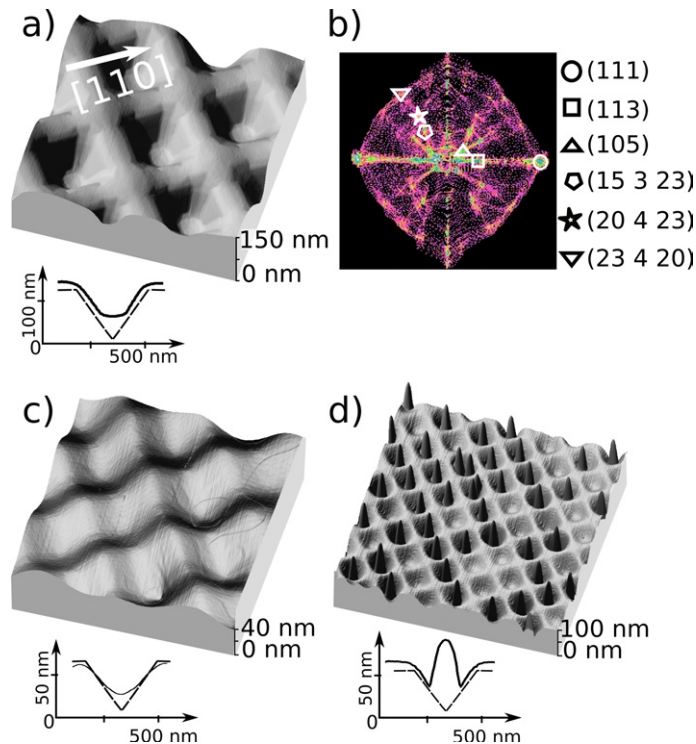


Figure 3. 3D $1 \times 1 \mu\text{m}^2$ AFM images of $\{111\}$ pit-patterned substrates with pit period 350 nm after (a) 2.9 ML of Ge grown at 700°C , complemented by the corresponding facet evaluation plot (b) [34]. 3D $1 \times 1 \mu\text{m}^2$ AFM images of $\{111\}$ pit-patterned substrates with pit period 350 nm after (c) 4.8 ML Ge grown at 700°C . (d) 3D $5 \times 5 \mu\text{m}^2$ AFM image after the growth of 4.8 ML Ge at 700°C using a substrate with 400 nm pit period. The schematic cross sections below the AFM images show the pit facets after etching (dashed line) and an AFM line scan after Ge growth.

$\{111\}$ pits to those obtained after RIE etching. Evidently, for these growth parameters, there is no obvious benefit in using $\{111\}$ pits as nucleation centers.

3. Conclusion

We have shown that on $\{001\}$ Si substrates patterned by inverted $\{111\}$ faceted pyramids, the ordered growth of SiGe islands is possible. The resulting islands show the largest aspect ratio so far observed for ordered SiGe islands. However, even at low growth temperatures around 550°C , strong intermixing during Ge deposition is observed, as evidenced by an island aspect ratio smaller than the ideal one for $\{111\}$ inverted pyramids (0.7) as well as by the photon energy of the island PL. Energy level calculations show that a unique electronic configuration with largely enhanced overlap between the hole ground state and Δ_{xy} wave functions can be realized by SiGe island growth in $\{111\}$ faceted pits. At elevated Ge growth temperatures, we observe that a small Ge coverage induces a large amount of Si transfer into the pits, effectively smoothing the surface towards a $\{111\}$ faceted one.

Acknowledgments

This work was supported by the Austrian Science foundation FWF under project F2512-N08, the ‘Austrian Gesellschaft für Mikro- und Nanoelektronik’, and by the Italian CARIPLO foundation under project ‘MANDIS’.

References

- [1] Mo Y W, Savage D E, Swartzentruber B S and Lagally M G 1990 *Phys. Rev. Lett.* **65** 1020
- [2] Stangl J, Holý V and Bauer G 2004 *Rev. Mod. Phys.* **76** 725
- [3] Berbezier I and Ronda A 2009 *Surf. Sci.* **64** 47
- [4] Zhong Z and Bauer G 2004 *Appl. Phys. Lett.* **84** 1922
- [5] Chen G, Vastola G, Lichtenberger H, Pachinger D, Bauer G, Jantsch W, Schäffler F and Miglio L 2008 *Appl. Phys. Lett.* **92** 113106
- [6] Grützmacher D *et al* 2007 *Nano Lett.* **7** 3150
- [7] Dorsch W, Steiner B, Albrecht M, Strunk H P, Wawra H and Wagner G 1998 *J. Cryst. Growth* **183** 305
- [8] Yang B, Liu F and Lagally M G 2004 *Phys. Rev. Lett.* **92** 025502
- [9] Brehm M *et al* 2009 *Phys. Rev. B* **80** 205321
- [10] Krishna S, Sabarinathan J, Linder K and Bhattacharya P 2000 *J. Vac. Sci. Technol. B* **18** 1502
- [11] Lee H, Johnson J A, He M Y, Speck J S and Petroff P M 2000 *Appl. Phys. Lett.* **78** 1
- [12] Kim E S, Usami N and Shiraki Y 1998 *Appl. Phys. Lett.* **72** 1617
- [13] Schmidt O G, Jin-Phillipp N Y, Lange C, Denker U, Eberl K, Schreiner R, Grabeldinger H and Schweizer H 2000 *Appl. Phys. Lett.* **77** 4139
- [14] Sanduijav B, Matei D, Chen G and Springholz G 2009 *Phys. Rev. B* **80** 125329
- [15] Zhong Z, Chen P, Jiang Z and Bauer G 2008 *Appl. Phys. Lett.* **93** 043106
- [16] Dais C, Mussler G, Sigg H, Fromherz T, Auzelyte V, Solak H H and Grützmacher D 2008 *Europhys. Lett.* **84** 67017
- [17] Kapon E, Pelucchi E, Watanabe S, Malko A, Baier M, Leifer K, Dwir B, Michelini F and Dupertuis M 2004 *Physica E* **25** 288
- [18] Biasiol G, Gustafsson A, Leifer K and Kapon E 2002 *Phys. Rev. B* **65** 205306
- [19] Dais C, Solak H H, Müller E and Grützmacher D 2008 *Appl. Phys. Lett.* **92** 143102
- [20] Sato K, Shikida M, Yamashiro T, Asaumi K, Iriye Y and Yamamoto M 1999 *Sensors Actuators* **73** 131
- [21] Stoffel M, Kar G S, Denker U, Rastelli A, Sigg H and Schmidt O G 2004 *Physica E* **23** 421
- [22] Chen G, Lichtenberger H, Bauer G, Jantsch W and Schäffler F 2006 *Phys. Rev. B* **74** 035302
- [23] Zhang J J, Stoffel M, Rastelli A, Schmidt O G, Jovanovic V, Nanver L K and Bauer G 2007 *Appl. Phys. Lett.* **91** 173115
- [24] Lu G H, Cuma M and Liu F 2005 *Phys. Rev. B* **72** 125415
- [25] Montalenti F, Marzegalli A, Capellini G, De Seta M and Miglio L 2007 *J. Phys.: Condens. Matter* **19** 225001
- [26] Stoffel M, Rastelli A, Tersoff J, Merdzhanova T and Schmidt O G 2006 *Phys. Rev. B* **74** 155326
- [27] Dashiell M W, Denker U, Müller C, Costantini G, Manzano C, Kern K and Schmidt O G 2002 *Appl. Phys. Lett.* **80** 1279
- [28] Majewski J A, Birner S, Trellakis A, Sabathil M and Vogl P 2004 *Phys. Status Solidi C* **1** 2003
- [29] Brehm M, Suzuki T, Fromherz T, Zhong Z, Hrauda N, Hackl F, Stangl J, Schäffler F and Bauer G 2009 *New J. Phys.* **11** 063021
- [30] Winkler R, Merkler M, Darnhofer T and Rössler U 1996 *Phys. Rev. B* **53** 10858
- [31] Fromherz T, Meduňa M, Bauer G, Borak A, Falub C, Tsujino S, Sigg H and Grützmacher D 2005 *J. Appl. Phys.* **98** 044501
- [32] Schüllli T U *et al* 2009 *Phys. Rev. Lett.* **102** 025502
- [33] Lutz M A, Feenstra R M, Mooney P M, Tersoff J and Chu J O 1994 *Surf. Sci.* **316** L1075